

OPTIMIZATION OF FLUID DYNAMICS BY SHEAR THINNING IN STIRRED TANKS USING ANCHOR STIRRERS WITH CONVERGENT HOLLOWES

Abderrahim Sidi Mohammed Nekrouf¹  [0009-0007-9160-4406], Sarra Youcefi^{2*}  [0000-0001-5156-6432] and Mohamed Bouzit³  [0000-0002-1417-7291]

¹ Laboratory of Applied Mechanics, University of Sciences and Technology of Oran, 1505 El Mnaouer, Oran, 31000, Algeria
e-mail: abderrahimmohammed.nekrouf@univ-usto.dz

² Department of Mechanical Engineering, University of Sciences and Technology of Oran, 1505 El Mnaouer, Oran, 31000, Algeria
e-mail: sarra.youcefi@univ-usto.dz

³ Laboratory of Maritime Sciences and Engineering, University of Sciences and Technology of Oran, 1505 El Mnaouer, Oran, 31000, Algeria
e-mail: Bouzit_mohamed@yahoo.fr

*corresponding author

Abstract

Agitator shapes are of paramount importance in mixing processes, prompting researchers to explore new configurations to improve these operations. Our study focuses on the three-dimensional fluid dynamics in a flat-bottomed cylindrical tank equipped with different anchor shapes, ranging from the standard configuration to modified variants. Using both Newtonian and non-Newtonian fluids under laminar conditions, we aim to assess the impact of these variations on agitation performance. To analyze these data, we have defined ranges of parameters, including hydrodynamic parameters such as Reynolds number, covering a range from 1 to 100, as well as the rheological behavior index, varying from 0.6 to 1.4. In addition, we are exploring the influence of the number of convergent hollowes. The new agitators equipped with convergent hollowes have generated axial and radial velocities approaching the tangential velocity, thereby promoting a more uniform distribution of fluids in the tank. This configuration thus facilitates a more homogeneous and efficient mixing. Additionally, energy consumption remains practically constant, offering advantages in terms of efficiency.

Keywords: Modeling, impeller tank, anchor stirrer, convergent hollow, shear thinning fluid, fluid dynamics, power number.

1. Introduction

Mechanical agitation systems play a central role in multiple industrial and scientific sectors, providing an effective solution for mixing, homogenizing, and dispersing liquid or solid materials within liquid mediums. Their relevance extends across a wide range of applications, from chemistry and biotechnology to the pharmaceutical and agro-food industries. Due to the vital

importance of agitation, the numerical and experimental analysis of hydrodynamic behavior in agitated tanks represents a valuable opportunity to identify and address potential issues. This study is of particular interest to researchers working in various industrial sectors (Sahu et al. 1999; Nienow and Miles 1978; Papastefanos and Stamatoudis 1989).

In the industry, agitated tanks of various shapes, equipped with simple or complex agitators, are commonly used. The design and modification of agitators are essential aspects of mixing systems, extensively explored by numerous research laboratories worldwide. In recent years, a significant portion of mechanical agitation research has focused on the hydrodynamic analysis of flow and energy consumption within agitated tanks. Researchers strive to enhance these aspects by making geometric modifications to both the agitators and tanks. Triveni et al. (2010) carried out experimental investigations into the flow dynamics within a tank fitted with an anchor. They observed an increase in the proportion of well-mixed surface area as the speed of the wheel increased, regardless of whether the systems were Newtonian or non-Newtonian. Bouzit et al. (2006) and Youcefi et al. (2023) conducted a numerical study in a tank containing a Newtonian fluid, stirred by a two-blade agitator. Their study confirmed that such configurations primarily generate tangential flow. On the other hand, the second agitator produced more significant axial and radial velocity profiles. Ameur et al. (2018) innovated by designing a new blade configuration aimed at reducing energy consumption while improving mixing quality. Their studies examined the effects of curvature, diameter, and the number of blades. The results showed that curved blades are more effective in reducing energy consumption than straight blades. Devi and Kumar (2015) found that an agitated tank using a curved-blade turbine is more efficient than a Rushton turbine. Luan et al. (2017) used a new curved six-blade turbine to improve mixing time and energy consumption, noting that the mixing rate and efficiency are influenced by the turbine's eccentricity and clearance from the bottom of the tank. Distelhoff and Marquis (2000) observed that the concentration is concentrated in the planes above and below for the Rushton turbine with inclined blades. Boonkanokwong et al. (2018) conducted an experimental study of granular materials circulating in a cylindrical-blade turbine agitator, analyzing different blade configurations and material properties affecting torque and power. They showed that the average torque over time depended on the number of turbine blades.

Other researchers have made significant improvements to agitation systems. Among these studies, some have focused on developing new forms of agitators: Foukrach et al. (2020), Ameur and Bouzit (2013) and Kamla et al. (2021) while others have explored the use of various types of baffles: Youcefi et al. (2013, 2023), Ammar et al. (2011), Foukrach and Ameur (2019) and Kamla et al. (2017). These modifications aim to enhance kinetic movement within agitated tanks while reducing energy consumption in various types of flows, whether turbulent or laminar.

The non-Newtonian fluids are the heart of recent advances in the field of mechanical agitation. In contrast to Newtonian fluids, their viscosity varies with applied stress. This unique characteristic opens up new perspectives for enhancing mixing, homogenization and dispersion processes. Woziwodzki et al. (2010) experimented with shear thinning fluids at various mass concentrations using three types of impellers. They noted that the mixing time is heavily influenced by both the number of agitators and the spacing between them. Rahmani et al. (2013) present an analysis of mechanical agitation of a viscoplastic fluid, following the Bingham law, with a tank equipped with a barrier agitator. This study observed that the complex fluid behavior varies over time, also leading to a quasi-immobilization of regions within the agitation system. Ameur et al. (2012) conducted a hydrodynamic study using a yield stress fluid with a Maxblend impeller in a tank. During their experimental study on a complex fluid stirred by a two-blade impeller in a tank, Youcefi and Youcefi (2015) demonstrated a significant dependence of the mixing time on the fluid's elasticity. Patel et al. (2012) carried out an experimental study on a pseudoplastic fluid in an agitated reactor using a Maxblend-type impeller. The results of this study show a significant improvement in mixing performance with the use of the Maxblend

impeller. Similarly, recent research has highlighted the importance of heat transfer for non-Newtonian fluids in agitated tanks. These studies, including: Mokhefi et al. (2021, 2023), Naik and Vinod (2018), Perarasu et al. (2012) and Alami et al. (2020) have provided a better understanding of heat transfer mechanisms in these complex systems, where the rheological properties of fluids play a pivotal role. By understanding how the viscosity and flow behavior of non-Newtonian fluids influence heat transfer, these advancements enable better design of industrial processes involving these fluids, thus contributing to more efficient energy use and improved quality of final products.

This study fills a gap in mechanical stirring research by focusing on anchor stirrers, which are often overlooked in the literature. It explores ways of improving hydrodynamic mixing and energy consumption, particularly for Newtonian and non-Newtonian fluids. The main objective is to design new agitator configurations that promote not only axial and radial mobility, but also tangential motion, thus presenting inventive strategies for boosting the energy efficiency of mixing procedures.

2. Description of the mixing system

Our setup consists of a cylindrical tank with a flat bottom of diameter D and height H . To agitate the fluid, it is necessary to introduce a rotating mechanical device with a rotational speed N in the form of an anchor, characterized by a predominant tangential flow and low radial and axial flow. This agitator has a diameter d , height h , blade length L , and thickness w . The location of this impeller C is between the base of the agitator and the bottom of the tank and attached to a central cylindrical shaft of diameter da . Refer to Fig. 1 for visualization. The geometric ratios in the agitation system are: $D = H$, $h/D = 0.9$, $d/D = 0.779$, $L/D = 0.074$, $C/D = 0.067$, $da/D = 0.025$, $w/D = 0.025$, $Lc/D = 0.18$ and $Lm/D = 0.09$.

The flow studied in our research is a shear-thinning fluid, with a density of 1394 kg m^{-3} and a viscosity of $8 \text{ Pa}\cdot\text{s}$ (Ameur and Bouzit 2013). The flow indices range from 0.6 to 1.4, indicating a range of different rheological behaviors.

For flow indices less than 1, this type of fluid is generally referred to as pseudo plastic fluids. These fluids exhibit a decrease in viscosity with increasing shear rate, meaning they flow more easily at higher shear rates. Conversely, for flow indices greater than 1, these fluids are called shear-thickening fluids.

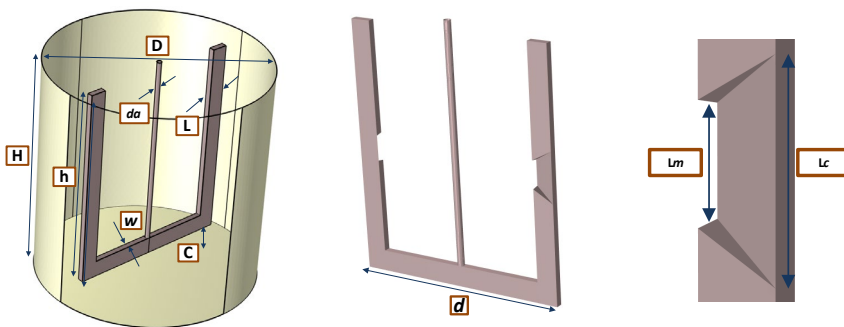


Fig. 1. Dimensions of the geometric configurations.

The modifications of the agitators are essential to handle both Newtonian and non-Newtonian fluids in order to improve the mixing process and obtain high-quality products. In this context, a new design has been developed to enhance the performance of the agitator. This design involves a specific convergent hollow placed within the anchor, with a cutting line Lc crossing the intersection of the front and right interface in the outer part of the anchor. It then extends with a digging to the intersection of the rear and left interface Lm , but this time in the inner part of the anchor. This configuration is positioned in the vertical half of the agitator, particularly in the section where the right blade of the anchor is located. This modification aims to maximize the efficiency of the agitator by increasing the radial movement of the fluid at this strategic point, thereby promoting better mixing and more homogeneous dispersion of components in the tank.

Additionally, this configuration is also applied to the other vertical half of the agitator to ensure symmetry in the mixing process. However, it is necessary to maintain the orientation of this convergent hollow due to the fluid circulation in this part (Fig. 2).

To enhance the distribution of our variation, we increased the quantity of convergent hollows n_c to ensure the continuous effect across the entire domain. In our study, we compared a standard anchor to one with a single convergent hollow and another with three such hollows to visualize the difference between these three forms. These distinct configurations are depicted in Fig. 2.

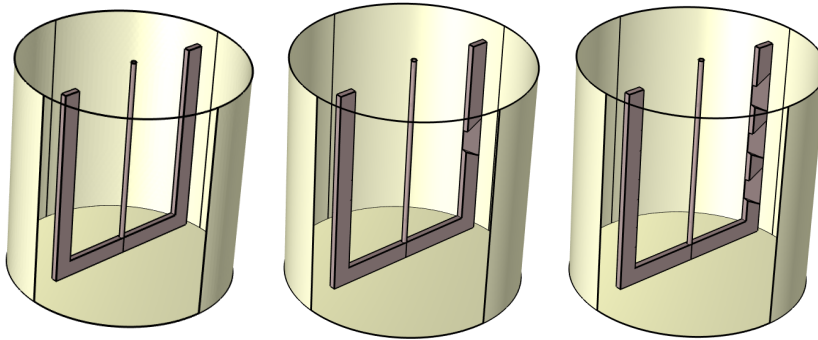


Fig. 2. Various designs of stirrers.

3. Mathematical model

The mathematical model of mechanical agitation in a purely laminar steady-state regime relies on the use of Cartesian coordinates (OXYZ), enabling a precise description of fluid flow dynamics within the agitated tank. The equilibrium equations governing the movement of non-Newtonian fluid are formulated based on these coordinates and are essential for understanding and predicting its behavior. These equations, solving a set of differential mathematical equations known as the Navier-Stokes equations, govern the flow inside the agitated tank equipped with the new anchor design. They include continuity equations, describing fluid mass conservation, and momentum conservation equations, governing its motion. The basic equations are as follows:

Mass balance:

$$\frac{\partial U}{\partial X} + \frac{\partial V}{\partial Y} + \frac{\partial W}{\partial Z} = 0 \quad (1)$$

Momentum balance:

$$\rho \left(U \frac{\partial U}{\partial X} + V \frac{\partial U}{\partial Y} + W \frac{\partial U}{\partial Z} \right) = -\frac{\partial P}{\partial X} + \frac{\partial \tau_{XX}}{\partial X} + \frac{\partial \tau_{XY}}{\partial Y} + \frac{\partial \tau_{XZ}}{\partial Z} \quad (2)$$

$$\rho \left(U \frac{\partial V}{\partial X} + V \frac{\partial V}{\partial Y} + W \frac{\partial V}{\partial Z} \right) = -\frac{\partial P}{\partial Y} + \frac{\partial \tau_{XY}}{\partial X} + \frac{\partial \tau_{YY}}{\partial Y} + \frac{\partial \tau_{YZ}}{\partial Z} \quad (3)$$

$$\rho \left(U \frac{\partial W}{\partial X} + V \frac{\partial W}{\partial Y} + W \frac{\partial W}{\partial Z} \right) = -\frac{\partial P}{\partial Z} + \frac{\partial \tau_{XZ}}{\partial X} + \frac{\partial \tau_{YZ}}{\partial Y} + \frac{\partial \tau_{ZZ}}{\partial Z} - \rho g \quad (4)$$

The velocity field (U , V , W) and pressure (P) represent the fluid's flow characteristics, while τ denotes the shear stress, which is defined as:

$$\tau_{ij} = 2\eta \varepsilon_{ij} \quad (5)$$

Within this equation framework, τ_{ij} and ε_{ij} notations are utilized to denote the tensors of viscous stress and deformation rate, respectively. Moreover, the symbol η is applied to represent the apparent dynamic viscosity of the fluid, which depends on the consistency coefficient m and the shear-thinning behavior index n . The formula employed to determine the viscosity η is as follows (Kefayati 2015):

$$\eta = m \dot{\gamma}^{n-1} \quad (6)$$

with $\dot{\gamma}$ representing the velocity gradient defined by (Kefayati 2015):

$$\dot{\gamma} = \sqrt{2 \left[\left(\frac{\partial U}{\partial X} \right)^2 + \left(\frac{\partial V}{\partial Y} \right)^2 + \left(\frac{\partial W}{\partial Z} \right)^2 \right] + \left(\frac{\partial U}{\partial Y} + \frac{\partial V}{\partial X} \right)^2 + \left(\frac{\partial U}{\partial Z} + \frac{\partial W}{\partial X} \right)^2 + \left(\frac{\partial V}{\partial Z} + \frac{\partial W}{\partial Y} \right)^2} \quad (7)$$

For the behavior of non-Newtonian fluids, the Reynolds number (Re) varies as a function of the behavior index n and rotational speed N . Its definition is as follows (Ameur and Bouzit 2013):

$$\text{Re} = \frac{\rho N^{2-n} d^2}{m} \quad (8)$$

Due to the fact that tangential, radial, and axial velocities play a fundamental role in interpreting agitation systems, they are utilized in our study. Derived from Cartesian velocities U , V , and W , the tangential and radial velocities, as well as the axial velocity, are expressed as follows:

$$V_{\theta} = \frac{-UY + VX}{\sqrt{X^2 + Y^2}}, \quad V_r = \frac{UX + VY}{\sqrt{X^2 + Y^2}} \quad \text{and} \quad V_z = W \quad (9)$$

To provide a general analysis of the theoretical results, it was deemed necessary to introduce a non-dimensional quantity for the velocity components and spatial coordinates. Therefore, the velocities as well as the radial (R) and axial (Z) coordinates are transformed into their non-dimensional form in the following equations:

$$(V_{\theta}^*, V_r^*, V_z^*) = \frac{(V_{\theta}, V_r, V_z)}{\pi ND} \quad \text{and} \quad R^* = \frac{2R}{D}, \quad Z^* = \frac{2Z}{D} \quad (10)$$

The energy consumption by the agitation device can be estimated from the results of computational fluid dynamics. Starting from the fluid viscosity and shear resistance, one can derive the electrical power required to overcome friction within the agitated fluid. Thus, based on viscous dissipation, this power, symbolized by P_{θ} , can be calculated as follows:

$$Po = \iiint_{\text{Vessel volume}} \eta Q_v \, dX \, dY \, dZ \quad (11)$$

In this context, Q_v represents the viscous dissipation function, calculated using the following formula:

$$Q_v = 2 \left[\left(\frac{\partial U}{\partial X} \right)^2 + \left(\frac{\partial V}{\partial Y} \right)^2 + \left(\frac{\partial W}{\partial Z} \right)^2 \right] + \left(\frac{\partial U}{\partial Y} + \frac{\partial V}{\partial X} \right)^2 + \left(\frac{\partial U}{\partial Z} + \frac{\partial W}{\partial X} \right)^2 + \left(\frac{\partial V}{\partial Z} + \frac{\partial W}{\partial Y} \right)^2 \quad (12)$$

The power number is calculated using the following formula (13), providing a dimensionless representation of the consumed power.

$$N_p = \frac{Po}{\rho N^3 d^5} \quad (13)$$

Boundary conditions define the behavior of a solution at the boundaries of a domain and are essential for solving equations that model a physical phenomenon in a given space. The boundary conditions used to solve governing equations include the rotational velocity at the impeller wall and the no-slip condition at the cylindrical tank wall. These conditions are:

- Stirrer wall: $V_\theta = \pi N r$, $V_r = V_z = 0$;
- cylindrical tank walls: $V_\theta = V_r = V_z = 0$.

3. Numerical methods

Numerical detail: The finite element method, associated with Galerkin's discretization, is used to numerically solve partial differential equations. It involves projecting the base equation onto the test function space and integrating over the domain to obtain a system of discrete equations to solve. This approach approximates the solution of a physical problem by using simple functions in each finite element. In this work, we utilize the MRF (Multiple Reference Frame) technique to model flows around rotating geometries, such as our agitator in a tank. This method divides the computational domain into two zones: a rotating zone containing our agitator and a stationary zone containing the rest of the tank. It simplifies the resolution of the Navier-Stokes equations with boundary conditions, which is important for finding solutions when the agitation devices do not have a cylindrical shape. The mesh is primarily tetrahedral and refined at the boundaries of the tank wall, especially at those of the wheel due to our specific modification located in this region (Fig. 3).



Fig. 3. Explored mesh structure of the computational domain.

Mesh check: To guarantee the coherence of the results obtained in our study, regardless of the mesh configuration used or the number of elements, various mesh configurations have been explored. This approach aims to enhance the reliability of our analyses by ensuring close agreement with results already documented in the existing literature. To increase the precision of our results, we have chosen to use three different meshes (M1-M3). Table 1 presents variations in the global agitation power number (N_p), as well as the tangential, radial, and axial dimensionless velocities at the location ($X^* = 0.75$, $Y^* = 0$, $Z^* = 0.16$) for different numbers of elements. Our analysis focused on the mesh with 734772 elements (mesh M2), beyond which no significant variation was observed in the calculated values. The convergence criterion, defined by the relative error of each dependent variable, has been maintained below 10^{-6} . This approach aims to ensure result stability and eliminate any uncertainty related to mesh variations.

Mesh	M1	M2	M3
Elements	253627	734772	1033889
Power number	2.5255	2.5260	2.5262
Tangential velocity	0.3385	0.3241	0.3244
Radial velocity	0.0313	0.0332	0.0339
Axial velocity	0.0107	0.0103	0.0102

Table 1. Variation of the power number with dimensionless velocities in relation to the number of elements at $Re = 100$ and $n=1$.

Code validation: Before using our numerical model, it is imperative to validate its accuracy and reliability. To do this, we compared our results with experimental and numerical data available in the specialized literature, ensuring the consistency of our approach. In order to confirm our results, we adopted the same geometry parameters and flow conditions as those used in the experiments by (Bertrand 1983) and the numerical modeling by (Hami et al. 2008). We thus compared the tangential velocity as a function of the tank radius (Fig. 4), and we found a very good agreement, which consolidates the reliability of our numerical approach.

Table 2 illustrates the evolution of the power number as a function of Reynolds number for the present study, including references from (Bertrand 1983) and (Hami et al. 2008). The obtained results show a good level of reliability among the different data sets. It has been observed that the percentage difference between our numerical results and the other references for all Reynolds numbers does not exceed 5.38%, indicating that our numerical predictions exhibit a high degree of consistency and precision.

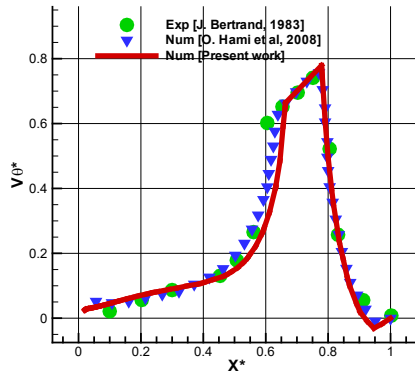


Fig. 4. Comparison of results obtained with those of the reference.

Reynolds Number	0.1	10	20
Present work	1500.17	16.007	8.54
Num (Bertrand 1983)	1468	15.99	9.026
Deviation (%)	2.19	0.10	5.38
Num (Hami et al. 2008)	1468.54	15.903	8.95
Deviation (%)	2.15	0.65	4.58

Table 2. Variation of the power number with dimensionless velocities in relation to the number of elements at $Re = 100$ and $n=1$.

3. Results and discussion

The modification of the agitator aiming to favor radial and axial flows while maintaining a predominant tangential flow is vital, as it influences various rheological behaviors of fluids, thus optimizing mixing processes and enhancing industrial operations' efficiency. In this study, we investigate the convergent effect of hollows in the anchor on the hydrodynamic and energetic behavior of the agitated tank. A detailed analysis is essential to understand the influence of the different graphic positions, and the use of a vertical plane to represent the results of our study (Fig. 5). All this is aimed at facilitating the visualization of the impact of the new design on the complex flow. The results are presented through 3D streamlines and velocity component contours, including tangential, axial, and radial velocity curves, as well as the power number to assess energy consumption. It is essential to mention the basic parameters considered in this study for a purely laminar system, including the Reynolds number Re ranging from 1 to 100, and the behavior index n ranging from 0.6 to 1.4, while considering different geometries.

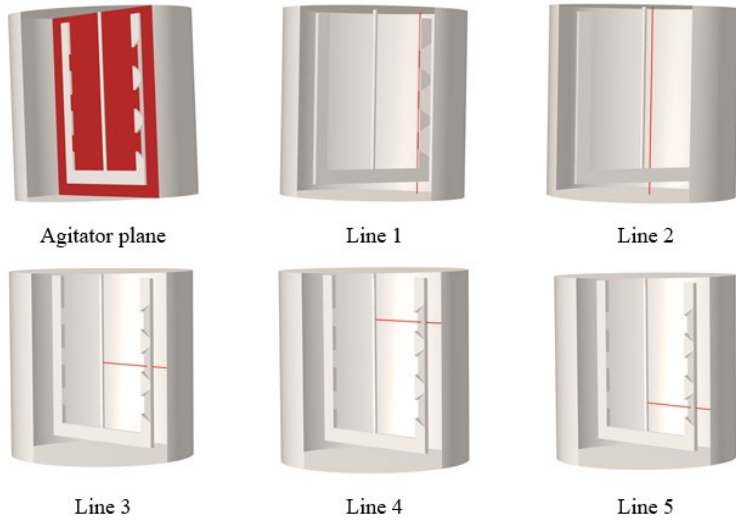


Fig. 5. Different measurements adopted in the present analysis.

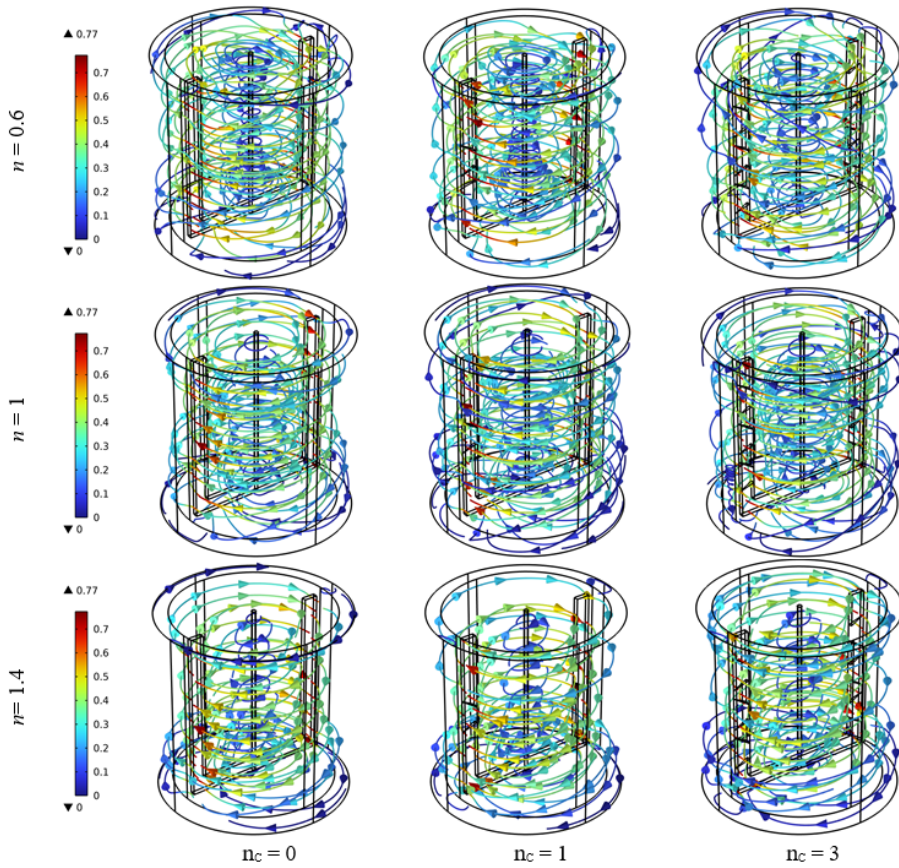


Fig. 6. Streamlines for different anchor geometries for various n .

Exploring the overall hydrodynamic performance: In this section, we examine two key factors: the configuration of the agitator equipped with a hollow convergent, and the behavior index in a mechanically stirred tank, and how they affect fluid movements and trajectory. Figure 6 presents the three-dimensional distribution of streamlines in the mixing system for different anchor configurations, including the standard configuration and modified variants, at a Reynolds number $Re=100$, with three behavior indices $n = 0.6, 1, \text{ and } 1.4$. The observation of the streamlines reveals that despite the increased size of vortices at the center of the tank, the tangential flow remains predominant for all configurations, even with different behavior indices. This finding underscores the significance of anchor design, as illustrated in Fig. 6. The incorporation of convergent hollows in the anchor intensifies turbulence and generates recirculation zones, resulting in more turbulent streamlines.

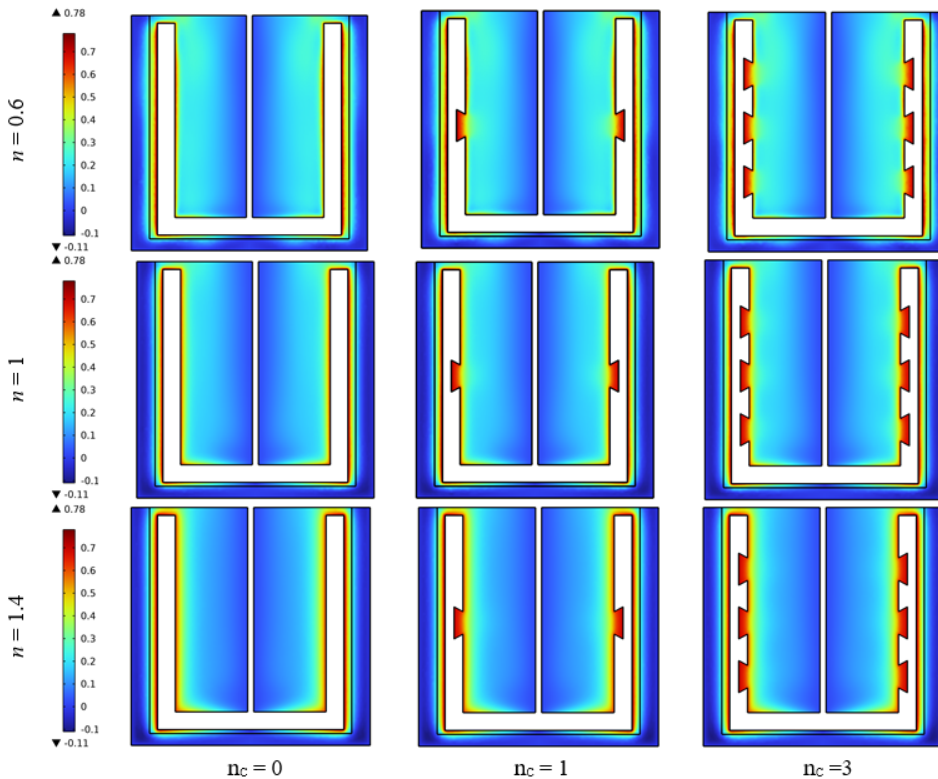


Fig. 7. Tangential velocity contours for different anchor geometries at the agitator plane for various n .

Figure 7 presents the contours of tangential velocity in the agitator plane of the tank, as illustrated in Fig. 5, for different anchor geometries with three different behavior indices: $n = 0.6, n = 1$ and $n = 1.4$, at a Reynolds number of $Re = 100$. Regardless of the behavior index, a high tangential velocity intensity is observed near the vertical anchor blade, creating a significant shear. The centrifugal force induced by the agitator rotation draws the fluid towards the periphery of the tank, reinforcing the tangential flow. In addition, a maximum tangential velocity field is formed in the convergent hollow of the anchor, consistent with the fact that the flow is in direct contact with the blade.

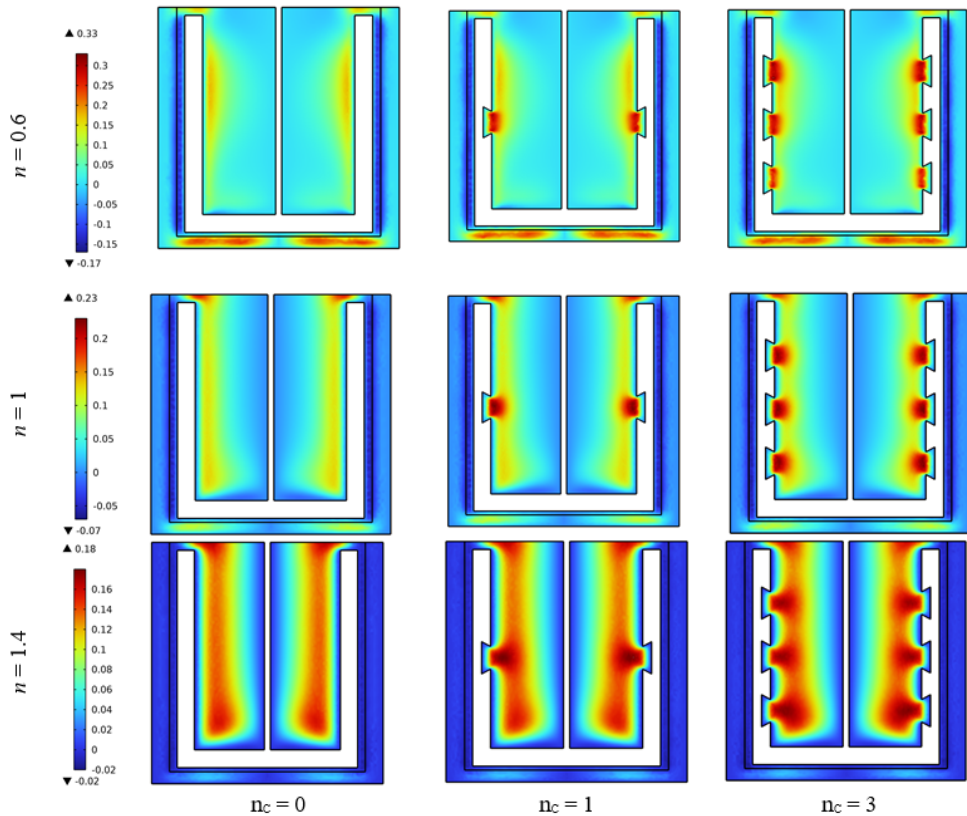


Fig. 8. Radial velocity contours for different anchor geometries at the agitator plane for various n .

Regarding radial velocity in Fig. 8, for a rheo-thinning fluid with a behavior index of $n = 0.6$, a significant radial velocity distribution is observed compared to other behavior indices, due to the shear effect resulting in decreased viscosity. This facilitates easier fluid flow and increases its velocity. Furthermore, a significant radial kinetic flux is observed near the outlet of the convergent hollow in the single convergent hollow anchor configuration. This is explained by the horizontally directed radial flow towards the convergent hollow. It is well known that velocity increases with the decrease in conduit surface, and this effect is similar for the other convergent hollows in the three convergent hollow configurations. The other behavior indices, $n = 1$ and $n = 1.4$, show similar trends, with the exception of the observed widening of the radial intensity at the exit of the trough, which converges with the increase in the behavior indices. This observation is attributed to the variation in viscosity induced by their rheological behavior. The last aspect to consider is the axial velocity distribution on the same plane. We observe a maximum intensity of axial velocity near the outlet of the convergent hollow. In the upper part of this outlet, the velocity field is negative, while in the lower part, it is positive, which is caused by recirculation zones. In the configuration with three convergent hollows, we observe that the third hollow contributed to a more pronounced increase in intensity at the bottom of the reservoir, particularly for the Newtonian and shear-thickening fluids, compared with the other convergent hollows (Fig. 9).

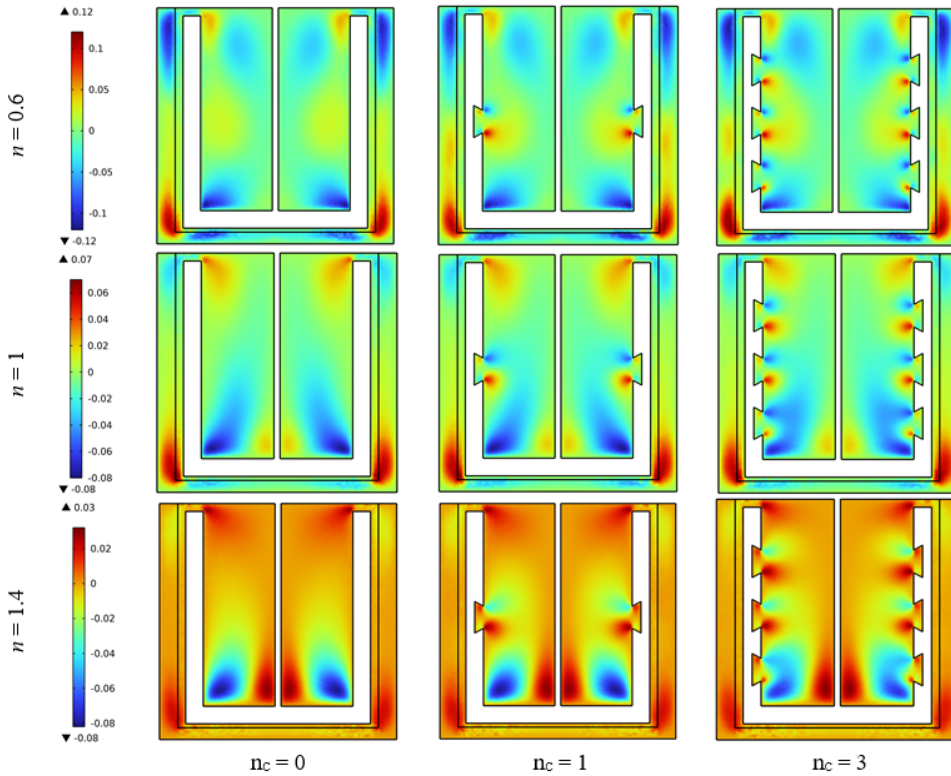


Fig. 9. Axial velocity contours for different anchor geometries at the agitator plane for various n .

Exploring the overall hydrodynamic performance: A clear and concise visual representation of trends is essential for understanding the impact of our anchor modification on various hydrodynamic behaviors in the stirred tank. This analysis focuses on variations in the three velocity components when the agitator geometry is altered. Tangential, radial, and axial velocities were examined along the lines in Fig.5, for three behavior indices $n = 0.6, 1, 1.4$, and a Reynolds number $Re = 100$. With regard to tangential velocity as shown in Fig. 10, an almost uniform distribution was observed along the different lines crossing the plane of the shaker. However, a slight decrease was noted along vertical line 1 at the exit of the convergent hollow compared to the standard anchor without hollows $n_c = 0$ for all three behavior indices. This decrease is attributed to the significant appearance of radial flow, which slows down tangential flow. This trend becomes more pronounced as the behavior index n is reduced. Horizontal lines 3, 4 and 5 show an increase in tangential velocity towards the center of the tank, followed by a decrease, attributed to convergent hollows decreasing as the behavior index n increases. Radial flow plays an important role in optimizing mixing when combined with tangential flow. In Fig. 11, which depicts the radial velocity along vertical line 1, a notable increase in radial velocity is observed followed by a reduction near the bottom of the tank for all configurations. Beyond this position, a very significant improvement is noticed for agitators modified with a hollow number of $n_c = 3$ compared to the standard shape $n_c = 0$ at the hollow positions.

This substantial variation is attributed to the circulation of this flow, which flows towards the convergent hollows until its exit, generating significant radial energy. This explanation applies to all hollow positions. All these variations decrease as the index n increases, just like the evolution

of tangential velocity. For line 2, an almost identical evolution is observed for all shapes and for any behavior index n . As for the rest of the lines, a significant radial flow is observed in the new configurations compared to the standard shape, on the horizontal line 3 a radial flow is created crossing the vertical blade on the path of the convergent hollow, while it is absent with the standard anchor in this region. Now, for the two horizontal lines (lines 4 and 5), which follow a similar trend to the previous line (line 3), we observe a predominant radial flow in the third shape, which has three hollows compared to the other shapes. This effect is due to the presence of these convergent hollows in the upper and lower parts. Moreover, this variation is reduced as a function of index n due to the rheological effect, as also shown in Fig. 10. It should be emphasized that, although axial flow is relatively less preponderant than the other flows, an insightful explanation of this essential component, as demonstrated by the streamlines in the figures, is essential to understand the benefits of this vertical flow with the new shapes used in our study. To enrich our understanding of this phenomenon, the curves presented in Fig. 12 offer an in-depth analysis of the third component of velocity, namely axial velocity. Despite the creation of this new shape with the aim of increasing the kinetic energy of the radial flow, we observed a growth in axial velocity in different regions, as revealed by the multiple lines used in our study. It is worth noting that the convergent hollow with an inclined perforation leads to an increase in axial velocity, as observed at the exit of the hollows (line 1) and in the center of the tank, particularly near the agitator shaft, with a significant improvement for a rheo-thickening fluid with high resistance, with a behavior index $n=1.4$ (line 2). As part of our research, we achieved a breakthrough in mixing by modifying the agitator shape and developing a new configuration to intensify radial flow. This adaptation also increased axial flow, while maintaining tangential flow. This significant development opens up new prospects for optimizing industrial processes and improving overall mixing efficiency.

Power consumption:

The power number is a parameter used in fluid dynamics to characterize the energy consumption of an agitator in a moving liquid. It is defined as the ratio between the agitator power and the fluid power and is used to assess the agitator's efficiency in mixing the fluid. Agitator power is influenced by various parameters, such as agitator rotation speed, fluid properties and tank design and dimensions. Reducing or conserving energy consumption is a major objective when it comes to optimizing energy performance.

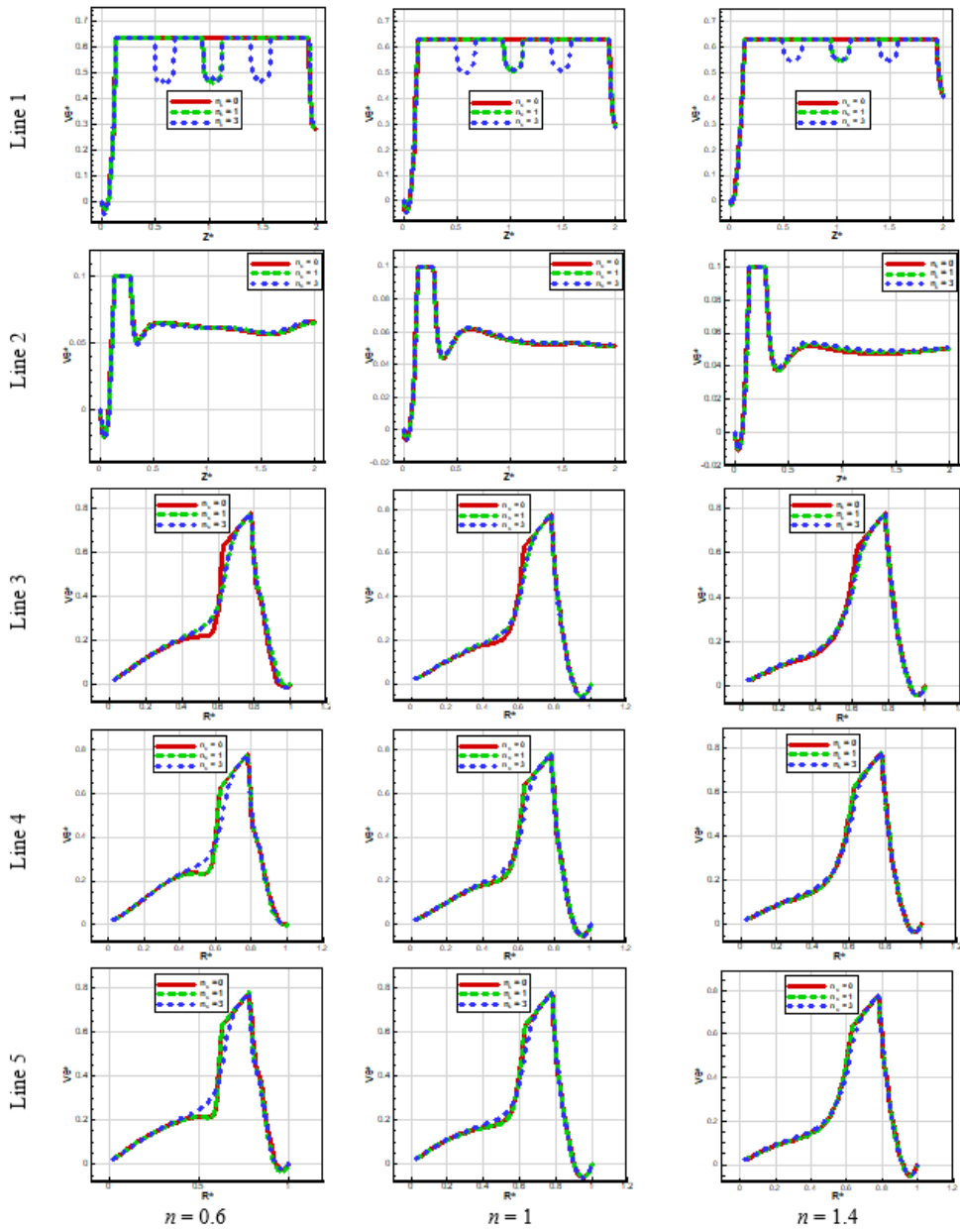


Fig. 10. Tangential velocity for different anchor geometries along different measurement lines for various n .

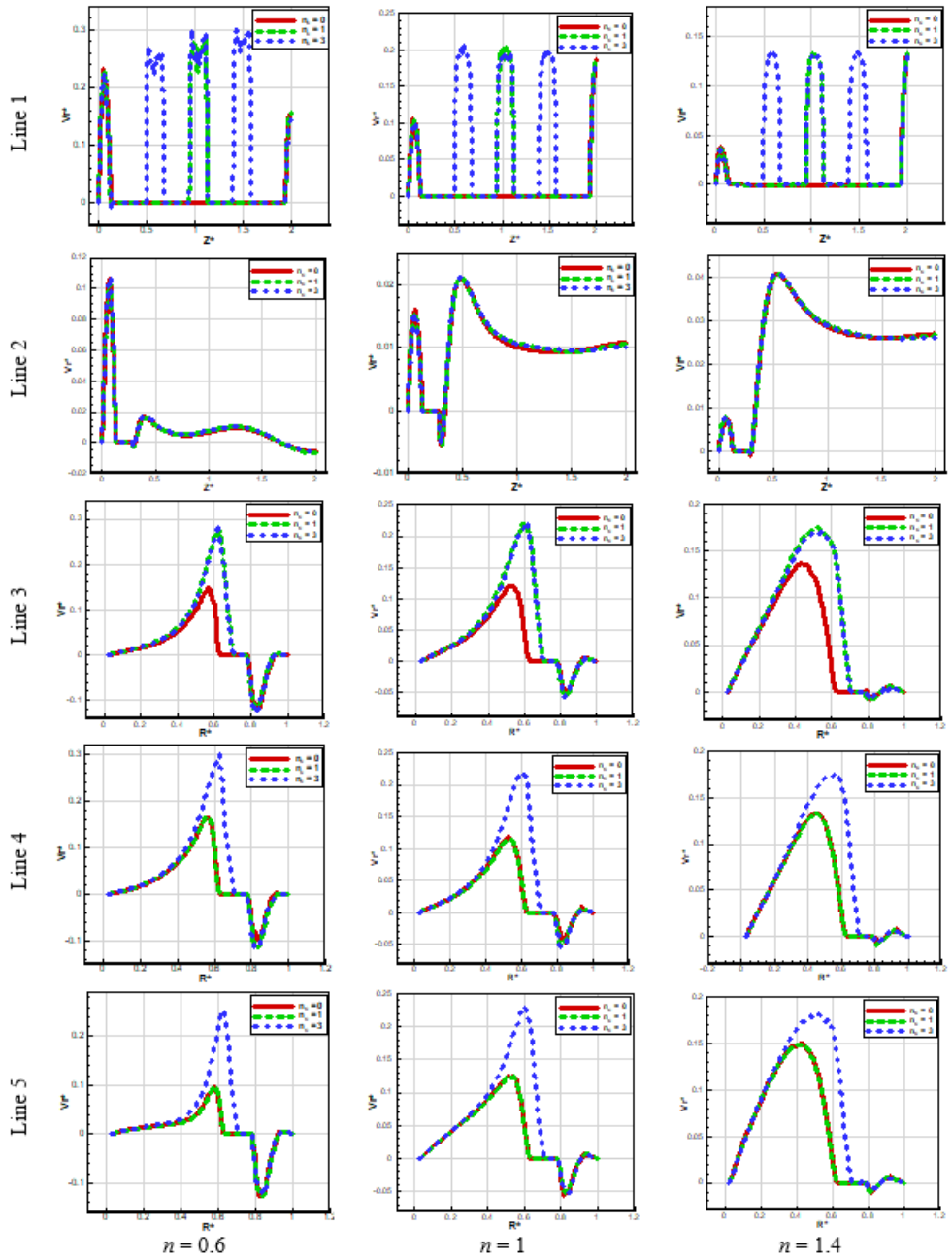


Fig. 11. Radial velocity for different anchor geometries along different measurement lines for various n .

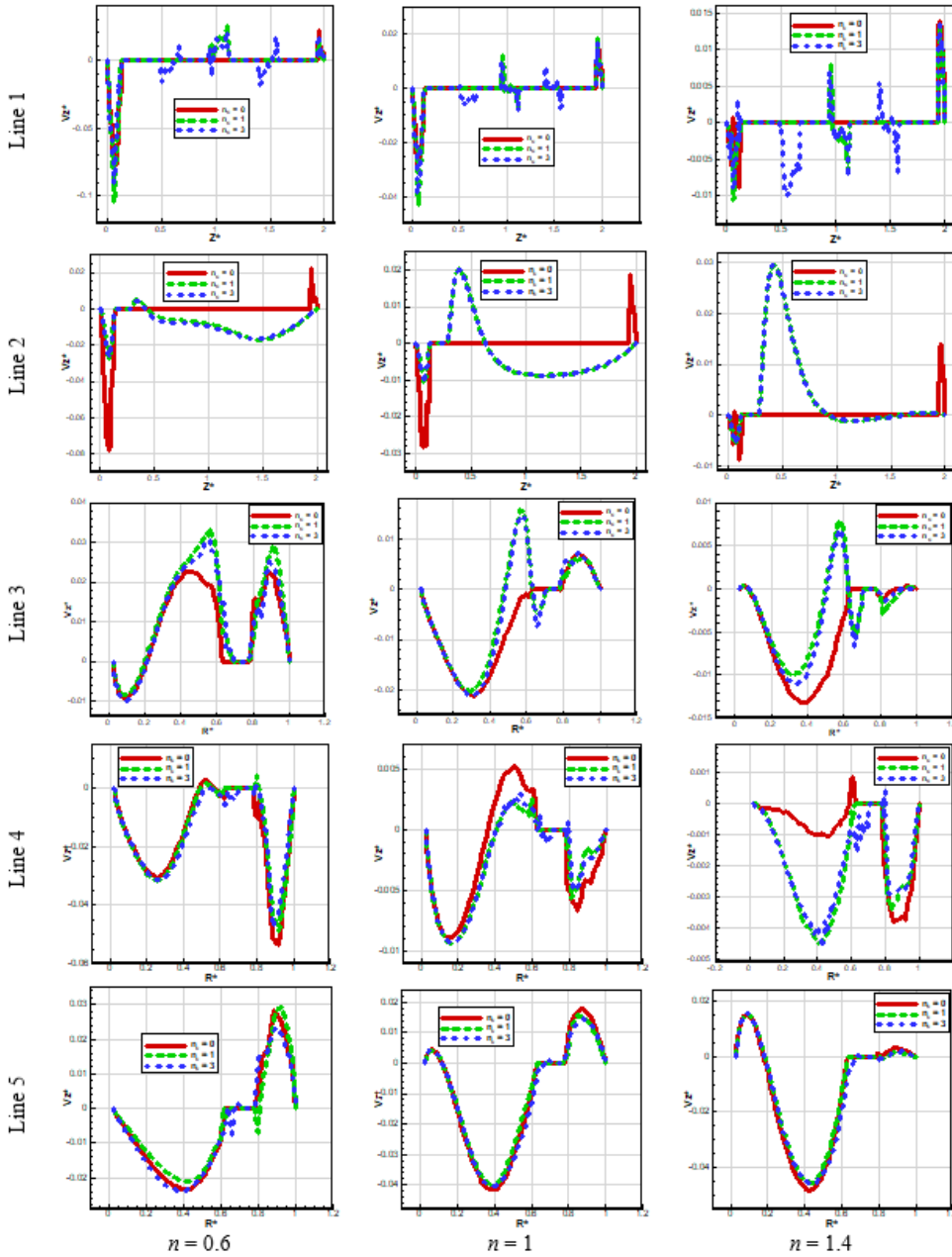


Fig. 12. Axial velocity for different anchor geometries along different measurement lines for various n .

Table 3 shows the variation of the power number for different behavior indices and Reynolds numbers for the new model with convergent hollows, including the standard shape. The results show a decrease in power number with the implementation of the new design, particularly for the configuration with three convergent hollows, as well as for different values of the behavior index.

This reduction demonstrates an optimization of energy efficiency. The numerical results confirm a decrease of up to 0.7779%, offering significant advantages for industrial applications.

N_p % N_p		$n_c = 0$	$n_c = 1$	$n_c = 3$
$Re=1$	$n=0.6$	58.66	58.52	58.26
		/	0,2386	0,6818
	$n=1$	177.65	177.19	176.36
		/	0,2589	0,7273
	$n=1.4$	547.56	546.07	543.3
		/	0,2721	0,7779
$Re=10$	$n=0.6$	6.533	6.524	6.509
		/	0,1377	0,3673
	$n=1$	18.54	18.50	18.44
		/	0,2157	0,5393
	$n=1.4$	55.22	55.08	54.81
		/	0,2535	0,7424
$Re=100$	$n=0.6$	1.162	1.161	1.160
		/	0,0860	0,1721
	$n=1$	2.531	2.528	2.526
		/	0,1185	0,1975
	$n=1.4$	6.660	6.652	6.642
		/	0.1201	0,2702

Table 3. Variation of the power number for different anchor geometries and Reynolds numbers.

4. Conclusions

A new design equipped with convergent hollows has been proposed to enhance the hydrodynamics of the impeller and optimize energy consumption in the agitated tank. These variations are observed in terms of velocity distribution, energy consumption, and mixing efficiency. The current results have led to several important conclusions:

Within this proposed new design, the stability of tangential velocity was observed, highlighting its persistent predominance in fluid dynamics within the agitated tank.

The new construction has significantly enhanced generation of axial and radial flow in the tank, resulting in a substantial increase in axial and radial velocity. This characteristic has a positive impact on mixing quality, which is particularly beneficial for suspensions.

The adoption of a new agitator design with convergent hollow has maintained energy efficiency, with a slight reduction in power numbers for both Newtonian and non-Newtonian fluids. This reduction in power decreases further with increasing Reynolds number, underscoring the importance of enhanced energy efficiency in operations at high flow rates. These findings confirm significant advantages, presenting an optimized solution for mixing processes.

For high behavior indices, a reduction in kinetic movement was observed, requiring higher energy consumption. This finding underscores the importance of considering fluid properties in the design of effective mixing equipment.

This study lays the groundwork for future research to delve deeper into the interactions between various agitator designs and fluid characteristics. Further experimental studies could validate simulation results and assist in refining agitator design models, thus paving the way for a more comprehensive and precise understanding and optimization of industrial mixing processes.

References:

- Alami AH, Abu Hawili A, Aokal K, Faraj M, Tawalbeh M (2020). Enhanced heat transfer in agitated tanks by alternating magnetic field stirring of aqueous Fe–Cu nanofluid, *Case Stud. Therm. Eng.*, 20, 100640.
- Ameur H, Bouzit M (2013). Numerical investigation of flow induced by a disk turbine in unbaffled stirred tank, *Acta Sci. Technol.*, 35(3), 469–476.
- Ameur H, Bouzit M, Helmaoui M (2012). Hydrodynamic study involving a Maxblend impeller with yield stress fluids, *J. Mech. Sci. Technol.*, 26(5), 1523–1530.
- Ameur H, Kamla Y, Sahel D (2018). Optimization of the operating and design conditions to reduce the power consumption in a tank stirred by a paddle impeller, *Period. Polytech. Mech. Eng.*, 62(4), 312–319.
- Ammar M, Driss Z, Chtourou W, Abid MS (2011). Effects of baffle length on turbulent flows generated in stirred tanks, *Cent. Eur. J. Eng.*, 1(4), 401–412.
- Bertrand J (1983). *Agitation de fluides visqueux. Cas de mobiles à pales, d'ancres et de barrières*, Thèse, Institut National Polytechnique de Toulouse, Toulouse.
- Boonkanokwong V, Frank RP, Valliappan P, Remy B, Khinast JG, Glasser BJ (2018). Flow of granular materials in a bladed mixer: effect of particle properties and process parameters on impeller torque and power consumption, *Adv. Powder Technol.*, 29(11), 2733–2752.
- Bouzit M, Benali L, Hachemi M, Bouzit F (2006). CFD simulations of the 3D velocity profile of paddle agitator and two-blade impeller in stirred tank with a highly viscous Newtonian fluid, *J. Appl. Sci.*, 6(13), 2733–2740.
- Devi TT, Kumar B (2015). Large-eddy simulation of turbulent flow in stirred tank with a curved blade impeller, *J. Eng. Thermophys.*, 24(2), 152–168.
- Distelhoff MFW, Marquis AJ (2000). Scalar mixing in the vicinity of two disk turbines and two pitched blade impellers, *Chem. Eng. Sci.*, 55(10), 1905–1920.
- Foukrach M, Ameur H (2019). Effect of baffles shape on the flow patterns and power consumption in stirred vessels, *SN Appl. Sci.*, 1(11), 1503.
- Foukrach M, Bouzit M, Ameur H, Kamla Y (2020). Effect of agitator's types on the hydrodynamic flow in an agitated tank, *Chin. J. Mech. Eng.*, 33, 1–18.
- Hami O, Draoui B, Mebarki B, Rahmani L, Bouanini M (2008). Numerical model for laminar flow and heat transfer in an agitated vessel by inclined blades anchor. *Proc. CHT-08 ICHMT International Symposium on Advances in Computational Heat Transfer, Marrakech, Morocco*, p. 19.

- Kamla Y, Ameer H, Arab MI, Azeddine B (2021). Data on the hydrodynamics and power consumption induced by modified anchor impellers in cylindrical tanks, *Data Brief*, 39, 107669.
- Kamla Y, Bouzit M, Ameer H, Arab MI, Hadjeb A (2017). Effect of the inclination of baffles on the power consumption and fluid flows in a vessel stirred by a Rushton turbine, *Chin. J. Mech. Eng.*, 30(4), 1008–1016.
- Kefayati GR (2015). Mesoscopic simulation of mixed convection on non-Newtonian nanofluids in a two-sided lid-driven enclosure, *Adv. Powder Technol.*, 26(2), 576–588.
- Luan D, Zhang S, Wei X, Duan Z (2017). Effect of the 6PBT stirrer eccentricity and off-bottom clearance on mixing of pseudoplastic fluid in a stirred tank, *Results Phys.*, 7, 1079–1085.
- Mokhefi A (2023). Hydrodynamic and thermal performance analysis of an inclined anchor impeller designed for yield stress food mixing applications, *Food Bioprod. Process.*, 143, 255–270.
- Mokhefi A, Bouanini M, Elmir M, Spitéri P (2021). Effect of the wavy tank wall on the characteristics of mechanical agitation in the presence of a Al₂O₃-water nanofluid, *Metall. Mater. Eng.*, 27(3), 301–320.
- Naik BAK, Vinod AV (2018). Heat transfer enhancement using non-Newtonian nanofluids in a shell and helical coil heat exchanger, *Exp. Therm. Fluid Sci.*, 90, 132–142.
- Nienow AW, Miles D (1978). The effect of impeller/tank configurations on fluid-particle mass transfer, *Chem. Eng. J.*, 15(1), 13–24.
- Papastefanos N, Stamatoudis M (1989). Effect of impeller and tank size on impeller power number in closed tanks for Reynolds numbers between 40 and 65000, *Chem. Eng. Commun.*, 80(1), 69–79.
- Patel D, Ein-Mozaffari F, Mehrvar M (2012). Improving the dynamic performance of continuous-flow mixing of pseudoplastic fluids possessing yield stress using Maxblend impeller, *Chem. Eng. Res. Des.*, 90(4), 514–523.
- Perarasu VT, Arivazhagan M, Sivashanmugam P (2012). Heat transfer of TiO₂/water nanofluid in a coiled agitated tank with propeller, *J. Hydrodyn.*, 24(6), 942–950.
- Rahmani L, Mebarki B, Allaoua B, Draoui B (2013). Laminar flow characterization in a stirred tank with a gate impeller in case of a non-Newtonian fluid, *Energy Procedia*, 36, 418–427.
- Sahu AK, Kumar P, Patwardhan AW (1999). CFD modeling and mixing in stirred tanks, *Chem. Eng. Sci.*, 54(13–14), 2285–2293.
- Triveni B, Vishwanadham B, Madhavi T, Venkateshwar S (2010). Mixing studies of non-Newtonian fluids in an anchor agitated tank, *Chem. Eng. Res. Des.*, 88(7), 809–818.
- Wozniowzki S, Broniarz-Press L, Ochowiak M (2010). Transitional Mixing of Shear-Thinning Fluids in Tanks with Multiple Impellers, *Chem. Eng. Technol.*, 33(7), 1099–1106.
- Youcefi S, Bouzit M, Ameer H, Kamla Y, Youcefi A (2013). Effect of some design parameters on the flow fields and power consumption in a tank stirred by a Rushton turbine, *Chem. Process Eng.*, 34(2), 293–307.
- Youcefi S, Bouzit M, Youcefi A, Mokhefi A (2023). Effect of an Inclined Slots on the Power Consumption and Vortices Size in a Rushton Turbine Agitated Tank, *Chin. J. Mech. Eng.*, 36(1), 147.
- Youcefi S, Mokhefi A, Bouzit M, Youcefi A (2023). Energy-Efficient Design Optimization of Two-Bladed Agitators in Cylindrical Tanks, *Int. J. Heat Technol.*, 41(6).
- Youcefi S, Youcefi A (2015). Power consumption and mixing time in rheologically complex fluids by a two-bladed impeller, *J. Mech. Sci. Technol.*, 29(2), 543–548.